Molecular mechanism of activation of human musk receptors OR5AN1 and OR1A1 by (*R*)-muscone and diverse other musk-smelling compounds

Lucky Ahmed[a,1], Yuetian Zhang[b,1], Eric Block[c,2], Michael Buehl[d], Michael J. Corr[d], Rodrigo A. Cormanich[e], Sivaji Gundala[c], Hiroaki Matsunami[f,g], David O'Hagan[d,2], Mehmet Ozbil[a], Yi Pan[b], Sivakumar Sekharan[a], Nicholas Ten[a], Mingan Wang[h], Mingyan Yang[d,h], Qingzhi Zhang[d], Ruina Zhang[b], Victor S. Batista[a,2], and Hanyi Zhuang[b,i,2]

[a]Department of Chemistry, Yale University, New Haven, CT 06520; [b]Department of Pathophysiology, Key Laboratory of Cell Differentiation and Apoptosis of the Chinese Ministry of Education, Shanghai Jiao Tong University School of Medicine, 200025 Shanghai, People's Republic of China; [c]Department of Chemistry, University at Albany, State University of New York, Albany, NY 12222; [d]School of Chemistry, University of St. Andrews, North Haugh, KY16 9ST St. Andrews, Scotland; [e]Department of Organic Chemistry, Chemistry Institute, University of Campinas, Campinas, SP 13083-970, Brazil; [f]Department of Molecular Genetics and Microbiology, Duke University Medical Center, Durham, NC 27710; [g]Department of Neurobiology, Duke Institute for Brain Sciences, Duke University Medical Center, Durham, NC 27710; [h]Department of Applied Chemistry, College of Science, China Agricultural University, Haidian District, 100193 Beijing, People's Republic of China; and [i]Institute of Health Sciences, Shanghai Jiao Tong University School of Medicine/Shanghai Institutes for Biological Sciences of Chinese Academy of Sciences, 200031 Shanghai, People's Republic of China

Edited by Jerrold Meinwald, Cornell University, Ithaca, NY, and approved March 21, 2018 (received for review July 21, 2017)

Understanding olfaction at the molecular level is challenging due to the lack of crystallographic models of odorant receptors (ORs). To better understand the molecular mechanism of OR activation, we focused on chiral (*R*)-muscone and other musk-smelling odorants due to their great importance and widespread use in perfumery and traditional medicine, as well as environmental concerns associated with bioaccumulation of musks with estrogenic/antiestrogenic properties. We experimentally and computationally examined the activation of human receptors OR5AN1 and OR1A1, recently identified as specifically responding to musk compounds. OR5AN1 responds at nanomolar concentrations to musk ketone and robustly to macrocyclic sulfoxides and fluorine-substituted macrocyclic ketones; OR1A1 responds only to nitromusks. Structural models of OR5AN1 and OR1A1 based on quantum mechanics/molecular mechanics (QM/MM) hybrid methods were validated through direct comparisons with activation profiles from site-directed mutagenesis experiments and analysis of binding energies for 35 musk-related odorants. The experimentally found chiral selectivity of OR5AN1 to (*R*)- over (*S*)-muscone was also computationally confirmed for muscone and fluorinated (*R*)-muscone analogs. Structural models show that OR5AN1, highly responsive to nitromusks over macrocyclic musks, stabilizes odorants by hydrogen bonding to Tyr260 of transmembrane α-helix 6 and hydrophobic interactions with surrounding aromatic residues Phe105, Phe194, and Phe207. The binding of OR1A1 to nitromusks is stabilized by hydrogen bonding to Tyr258 along with hydrophobic interactions with surrounding aromatic residues Tyr251 and Phe206. Hydrophobic/nonpolar and hydrogen bonding interactions contribute, respectively, 77% and 13% to the odorant binding affinities, as shown by an atom-based quantitative structure–activity relationship model.

olfaction | odorant receptor | musk | quantum mechanics | molecular dynamics

Musks, secretions obtained from odor glands of the male musk deer and other animals, and their synthetic equivalents, have an "animalic" and sensual yet warm, smooth, and soft odor. They are used as base notes in the most sexually provocative perfumes, where they are greatly valued because of their persistence and ability to act as fixatives for other fragrances. Indeed, it is said that "there is no fragrance on the market that does not contain musk odorants" (1). The principal odorous component of musk deer (*Moschus moschiferus*) musk is the chiral 15-membered ring ketone (*R*)-muscone [(*R*)-**1**); *l*-muscone; (*R*)-methylcyclopentadecanone; Fig. 1], whose structure was first elucidated by Ruzicka in 1926 (2), and for which numerous syntheses have been reported (3–22). (*R*)-**1** has an odor detection threshold of 4.5 ng/L (6), which is lower than the threshold for (*S*)-muscone [(*S*)-**1**]. The 17-membered ring ketone civetone **12**, from the African civet (*Civettictis civetta*), has also played an important role in perfumes. Indeed, civet is even mentioned in Shakespeare's *King Lear*: "Give me an ounce of civet, good apothecary, to sweeten my imagination [*King Lear* IV, vi, 133]."

However, the rarity of the musk pods and the difficulties involved in the large-scale synthesis of macrocyclic compounds prevented their usage in perfumery and contributed to the advent of synthetic musks. Predating the identification of the macrocyclic components of natural musks of animal and plant origins, several nitromusks were synthesized serendipitously in the late 1800s (23). The nitromusks, musk ambrette, musk

Significance

While natural musk has been used for 2,000 years in perfumery, and in traditional medicine for its cardioprotective effects, its mode of activating odorant receptors (ORs) is unknown. ORs, G protein-coupled receptors (GPCRs), which constitute 40% of all pharmacophore receptors, are also expressed in nonolfactory tissues. Understanding the activation of ORs at the molecular level is challenging due to lack of crystallographic models. By combining site-directed mutagenesis with computational studies of human musk ORs involving 35 chiral and achiral muscone analogues, we propose structural models, including binding site prediction and responsible amino acid residues identification. Our studies of musk-responsive ORs should assist the study of the pharmacological effects of musks involving non-OR GPCRs.

Author contributions: L.A., Y.Z., E.B., D.O., V.S.B., and H.Z. designed research; L.A., Y.Z., M.J.C., R.A.C., M.O., Y.P., S.S., N.T., M.W., M.Y., Q.Z., and R.Z. performed research; L.A. and Y.Z. contributed new reagents/analytic tools; L.A., Y.Z., E.B., M.B., M.J.C., R.A.C., S.G., D.O., V.S.B., and H.Z. analyzed data; and L.A., Y.Z., E.B., R.A.C., H.M., D.O., Q.Z., V.S.B., and H.Z. wrote the paper.

The authors declare no conflict of interest.

This article is a PNAS Direct Submission.

[1]L.A. and Y.Z. contributed equally to this work.

[2]To whom correspondence may be addressed. Email: eblock@albany.edu, do1@st-andrews.ac.uk, victor.batista@yale.edu, or hanyizhuang@sjtu.edu.cn.

This article contains supporting information online at www.pnas.org/lookup/suppl/doi:10.1073/pnas.1713026115/-/DCSupplemental.

Published online April 9, 2018.

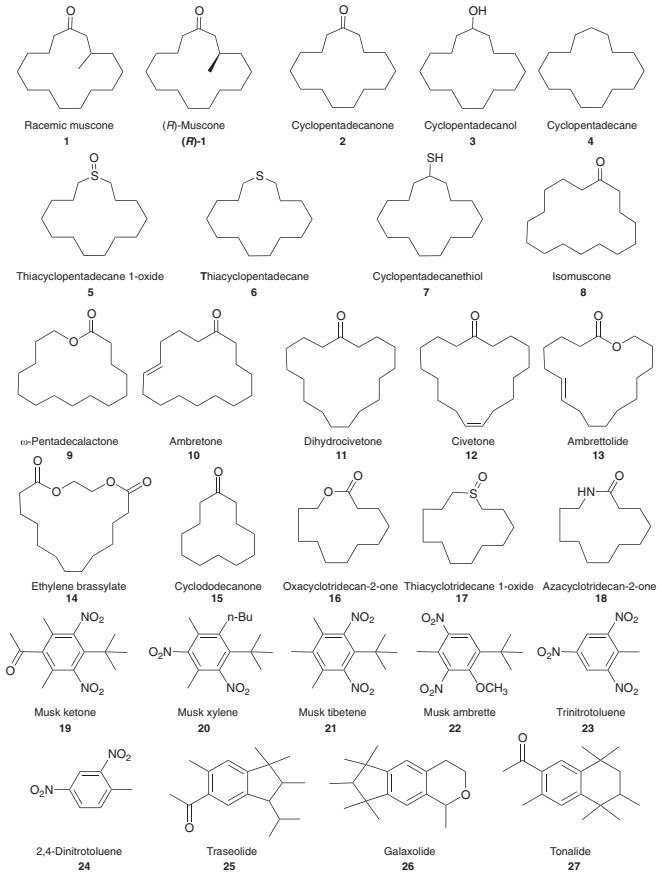

Fig. 1. Three classes of musk compounds and related compounds used in this study.

moskene, and musk tibetene, have long been known to be phototoxic and have been phased out of the cosmetic market. Musk ketone and musk xylene can still be used in Europe but with some restrictions because they are suspected of carcinogenic effects at high concentrations (24). With the discovery of polycyclic musks in the mid-20th century (1), synthetic musks have since enjoyed broad uses in the industry. While polycyclic musks dominate the global market, due to their lipophilic, persistent, and bioaccumulative nature, they are reported to accumulate in soil and sediments, raising environmental concerns (24) in view of their possible estrogenic/antiestrogenic effects (25).

Predating the synthesis of musk-smelling compounds, natural musk and its active constituent, (*R*)-**1**, have been widely used in traditional Chinese medicinal formulations. Natural musk is a valuable traditional Chinese medicine and has pharmacological effects promoting blood circulation and menstruation, inducing resuscitation, and possessing antiinflammatory activity. Some Chinese herbal medicines containing musk ingredient are widely used for treatment of stroke, dementia, inflammation, cerebral ischemia, coronary heart disease, injury, cancer, and other diseases (26–31). A recent study reported that muscone is one of the antiinflammatory constituents in a well-known traditional Chinese medicine named Pian-Tze-Huang (32). The antiinflammatory, antitumor, and antiinvasive effects of muscone are shared by other macrocyclic ketones such as civetone (33). In addition to these protective effects, musk compounds, including ambrettolide, muscone, and civetone, can stimulate the secretion of 17β-estradiol (34); together with its ability to promote blood circulation and menstruation, this makes musk a potent miscarriage-inducing agent (35). All of the above point to the existence of one or more drug targets mediating the pharmacological activities of musk compounds.

It has long been felt that only a few receptors are involved in sensing musk odor (36, 37). In recent studies, the odorant receptors (ORs) OR5AN1 and OR1A1 have been identified as human receptors for musk, including macrocyclic ketones as well as nitromusks (38–41). Understanding structure/function relationships responsible for ligand binding and activation of G protein-coupled receptors (GPCRs) (42, 43) remains an outstanding challenge of broad research interest, particularly given that some ORs expressed in cancer cell lines may contribute to tumorigenesis (44). ORs are members of the class A rhodopsin-like family of GPCRs (45, 46). Homology structural models of ORs can thus be based on crystallographic structures for rhodopsin-like receptors (47–51). The main challenge, however, is to provide experimental support for the proposed models for ligand–receptor interactions by site-directed mutagenesis and comparative analysis of ligand binding by biochemical measurements of receptor activation.

Given the historic significance of musks, whose use dates back more than 2,000 y, and their great economic importance to the fragrance industry (52) and in traditional medicine (32), here we examine the ligand-response profiles of OR5AN1 and OR1A1 and the binding sites for macrocyclic musks and nitromusks in homology structural models of OR5AN1 and OR1A1. We combine computational and experimental methods to validate the proposed model, including measurements of the receptor response upon ligand binding in conjunction with site-directed mutagenesis and calculations of ligand binding energies based on quantum mechanics/molecular mechanics (QM/MM) hybrid methods and ligand dynamics obtained via molecular dynamics (MD) simulations. We apply these methods to a broad range of conformationally diverse musk-related compounds including analogs of (*R*)-muscone containing a difluoromethylene (CF_2) group, for which X-ray structures are known, as well as the previously unknown 15-membered ring sulfoxide, in which the planar carbonyl group has been replaced with a pyramidal sulfinyl group.

Results and Discussion

Response of OR5AN1 to Various Musk Compounds. The musk smell of macrocyclic ketones has traditionally been associated with 14- to 18-carbon rings (1). Since there are perceptual and molecular similarities between natural and synthetic musk compounds, and if OR5AN1 is one of the few specific musk receptors in humans, could the same receptor also respond to structurally different nitromusks and polycyclic musks? A recent study found that in addition to macrocyclic musks OR5AN1 also showed a strong response to the nitromusks (38). In this study, we first explored the ligand selectivity of OR5AN1 by testing it against all three classes of musks and selected structurally related compounds (Fig. 1 and *SI Appendix*, Table S1). We found that, in addition to C15 and C16 macrocyclic carbonyl compounds, racemic muscone **1**, cyclopentadecanone **2**, isomuscone **8**, ω-pentadecalactone **9**, and ambretone **10** (38, 39, 41), OR5AN1 is also capable of responding to the C17 macrocyclic ketone compound, civetone **12**, and its hydrogenated analog dihydrocivetone **11**, but not to the structurally similar 17-membered ring lactones ambrettolide **13** or ethylene brassylate **14** (Fig. 2*A* and *SI Appendix*, Fig. S1*A* and Table S2). A previously unknown sulfur-containing analog (**5**) of cyclopentadecanone, containing a sulfinyl (S=O) group instead of a carbonyl group, as well as selected 12- and 13-membered ring counterparts (**15**–**18**) without a musk smell were also included for comparison. Of the three sulfur-containing analogs of cyclopentadecanone, thiacyclopentadecane 1-oxide **5**, thiacyclopentadecane **6**, and cyclopentadecanethiol **7**, only **5** activated OR5AN1 (Fig. 2*A* and *SI Appendix*, Table S2). Compound **5**, odorless at room temperature due to its low volatility,

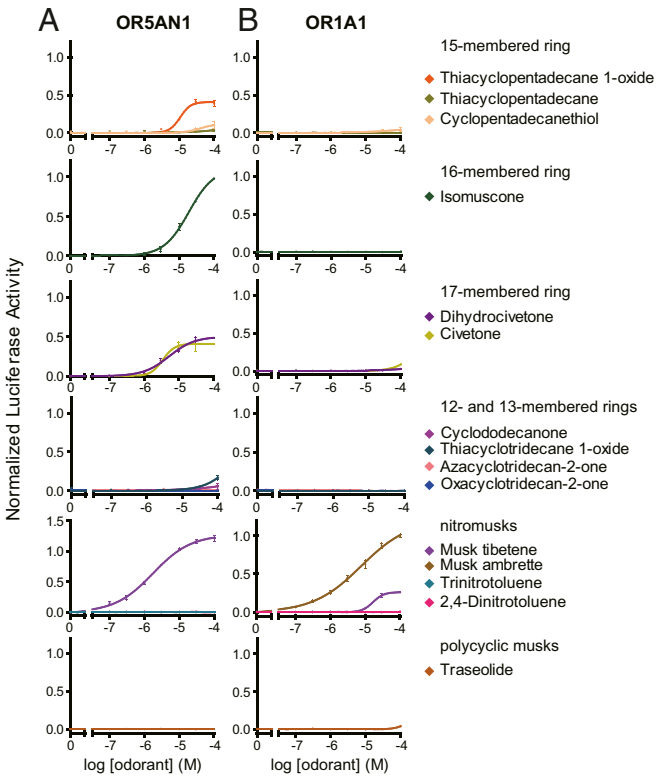

Fig. 2. Response of human musk receptors to various musk compounds. The response of the human musk receptors (*A*) OR5AN1 and (*B*) OR1A1 toward 12-, 13-, and 15- to 17-membered ring macrocyclic musks, nitromusks, and polycyclic musks. For all dose–response graphs, the *y* axis represents normalized luciferase activity ±SEM (n = 3). The responses of OR5AN1 are normalized to the highest value of racemic muscone **1**, and the responses of OR1A1 to musk ambrette **22**.

represents the first known sulfinyl musk. Interestingly, in contrast to carbonyl groups, the sulfinyl group is pyramidal at sulfur rather than planar.

Furthermore, the sulfinyl group absorbs at a very different region of the infrared spectrum compared with the carbonyl group (1,030–1,060 and 1,710–1,720 cm^{-1}, respectively), further arguing for the implausibility of the vibrational theory of olfaction (39). Thiacyclopentadecane itself has been reported to have "a very weak musky smell" which becomes more apparent on heating (53). Other divalent sulfur-containing musks are known as well (54–57). Consistent with previous reports (38, 39), cyclopentadecanol **3** induced a weak response while cyclopentadecane **4** failed to activate OR5AN1 (*SI Appendix*, Fig. S1*A* and Table S2). The above response profile underlines the importance of the sulfoxide group or the carbonyl group in the musk smell. The thiol or the sulfide group is not sufficient for ligand–receptor interaction. None of the 12- or 13-membered macrocyclic carbonyl compounds (**15**, **16**, and **18**) evoked a receptor response, while the previously unknown thiacyclotridecane 1-oxide **17** was very weakly responsive, consistent with their lack of musk smell (Fig. 2*A* and *SI Appendix*, Table S2). In addition, we compared the responses of racemic muscone **1** and (*R*)-**1**. Similar to the results in a previous study (38), the response to (*R*)-**1** is slightly better at high concentrations (*SI Appendix*, Fig. S2).

Nitromusks usually contain at least two nitro groups, as well as alkyl and/or tertiary alkyl groups, attached to a benzene ring. The disk-shaped structures of these molecules are reminiscent of the macrocyclic musks and may well fit into the same musk receptor binding pocket as the macrocycles. In addition to the two nitromusks, musk ketone **19** and musk xylene **20**, tested in a recent study (38), we also tested the structurally similar musk tibetene **21** and musk ambrette **22** against OR5AN1. Consistent with our hypothesis, the first three nitromusks strongly activated the receptor, with musk ketone **19** responding as sensitively as in the nanomolar ranges (Fig. 2*A* and *SI Appendix*, Fig. S1*A* and Table S2). In contrast, non-musk-smelling nitrobenzene compounds such as the symmetrical trinitrotoluene **23** and 2,4-dinitrotoluene **24** failed to activate the receptor (Fig. 2*A* and *SI Appendix*, Table S2). We note that the EC_{50} values for racemic muscone, musk tibetene, and musk xylene we obtained from the dose–response curves are similar to those previously reported (*SI Appendix*, Table S2). Finally, although some polycyclic musks (**25**–**27**) may share certain molecular similarities with the nitromusks, such as the central benzene ring, and the presence of substituent alkyl and alkoxy groups, none of the three polycyclic musks tested activated OR5AN1 (Fig. 2*A* and *SI Appendix*, Fig. S1*A* and Table S2). This lack of response points to the possible existence of other musk-responsive receptors in humans, at least those responding to the polycyclic musks.

Identification of a Second Human Musk OR. We next screened for additional human musk receptors by first focusing on the nitromusk, musk tibetene **21**. We found that, in addition to OR5AN1, OR1A1 emerged from the screen of the human receptor repertoire against musk tibetene (*SI Appendix*, Fig. S3). We then assayed the ligand selectivity of OR1A1. Unlike OR5AN1, which can respond to both macrocyclic and nitromusk compounds, OR1A1, an otherwise broadly tuned OR capable of responding to odorants of diverse structures (58), only responded prominently to selected nitromusks, namely musk ambrette **22**, and to a much lesser degree to the other nitromusks, but not to any of the macrocyclic or polycyclic musks (Fig. 2*B* and *SI Appendix*, Fig. S1*B* and Table S2). Thus, OR1A1 represents relatively narrower musk-related ligand tuning compared with OR5AN1. Another study also identified OR1A1 and additionally OR2J3 as human musk receptors that may partly contribute to the sensation of musk by responding to a few musk compounds (38).

Response of OR5AN1 to Fluorinated Musk Analogs. We have established that the stereoelectronic consequences of introducing a difluoromethylene (CF_2) group into a macrocycle results in a preference for the fluorine atoms to occupy corner locations (59), certainly in the lower energy conformers. This limits the conformational space that the ring system inhabits and has attractive prospects for exploring preferred agonist conformations of flexible rings. This approach has recently been explored by replacing a ring CH_2 by a CF_2 group to influence the odors of macrocyclic musk compounds, including cyclopentadecanone (60), musk lactones (61), civetone, and (*R*)-**1** (62). In particular, when the CF_2 group was inserted in different ring positions the odor intensity of (*R*)-muscone varied by human smell analysis (perfumery "nose" panel) (62). Here, we extend this analysis to investigate the response of the muscone receptor OR5AN1 to various CF_2-containing macrocyclic (*R*)-muscone analogs (compounds **28**–**37**, Fig. 3 and *SI Appendix*, Table S3).

We found that OR5AN1 showed varying responses to the saturated fluorinated analogs **28**–**31**, depending on the positions of the CF_2 substitution (Fig. 4 and *SI Appendix*, Table S4). Generally, the EC_{50} values were in the micromolar range, although only the C8 CF_2 muscone **30** gave a maximum agonist response at saturating concentrations and had the closest profile to (*R*)-**1** (Fig. 4, first row). We also assessed dehydro-musk ketones with double bonds and CF_2 groups at various positions. In general, the saturated and unsaturated analogs tested with the CF_2 at the same site respond similarly (**28**/**33**, **30**/**35**, and **31**/**37**).

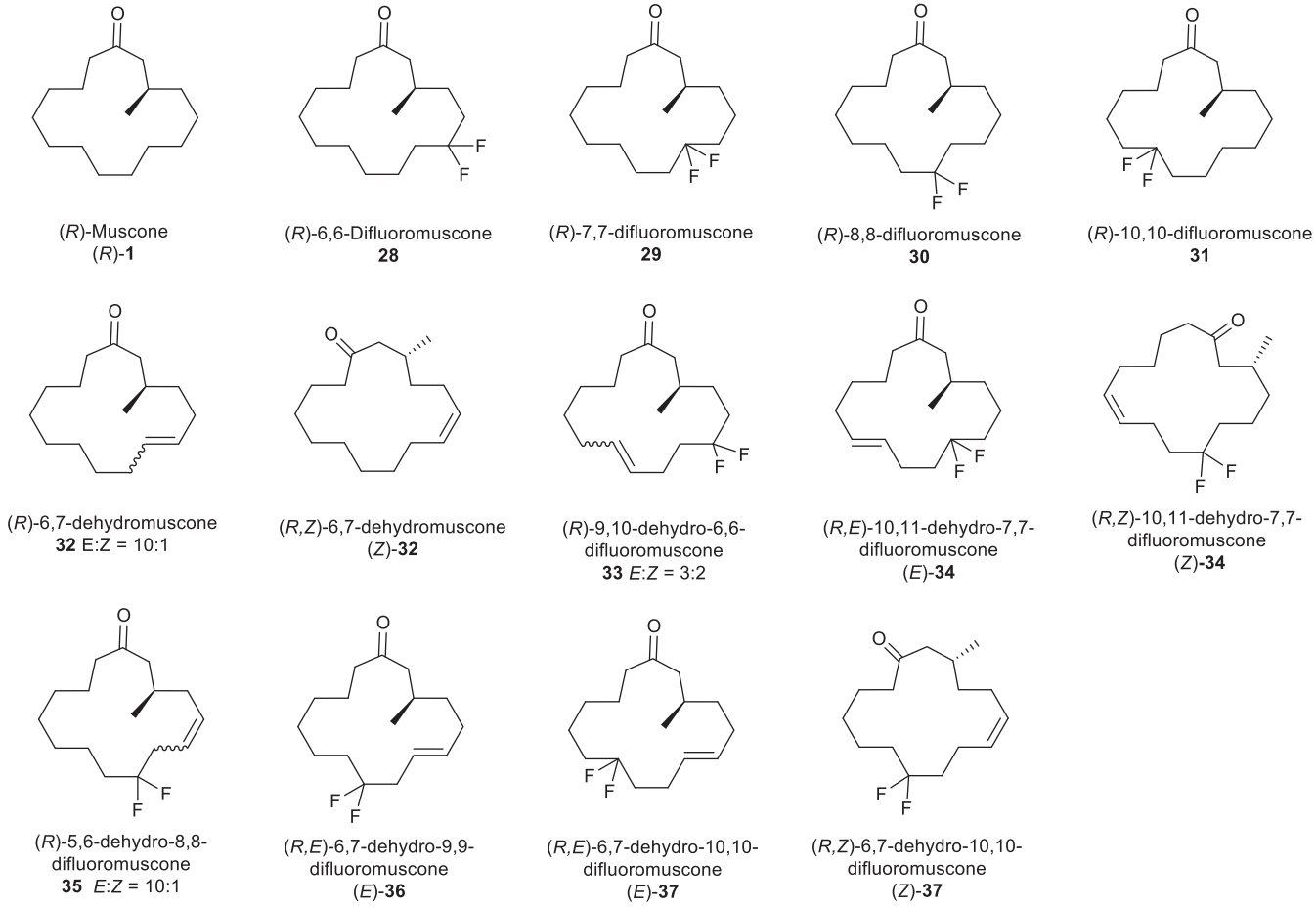

Fig. 3. Fluorinated musk compounds used in this study.

When both geometric isomers were available (**34** and **37**), the E isomer showed an increased potency compared with the Z isomer (Fig. 4). A notable exception is analog (*E*)-**34**, which exhibited a most intense and pleasant musky odor. Strikingly, (*E*)-**34** was three orders of magnitude more potent (EC_{50} 0.03 μM) than (*R*)-**1** (EC_{50} 19.9 μM) in the OR5AN1 assay and, similar to musk ketone (EC_{50} 0.02 μM), the most potent nitromusk. This is the muskiest musk ketone recorded on the OR5AN1 receptor using the in vitro assay. The combination of the 7-CF_2 group and the E double bond has a significant effect, presumably isolating ring conformations with optimal relevance for triggering the receptor. While (*E*)-**34** was not amenable to X-ray crystallography, the lowest energy calculated structures (*SI Appendix*, Fig. SA6, first row) are unusually elongated with the CF_2 at a corner and the double bond at an edge. This contrasts significantly with the lower energy conformers of the saturated CF_2-containing muscones **28–31** and that of the unsaturated (*Z*)-**34** (see Fig. 7 and *SI Appendix*, Figs. SA2–SA5). For example, the X-ray crystal structure (*SI Appendix*, Fig. SA7, first row) and an almost identical lowest energy calculated structure of (*Z*)-**34** (*SI Appendix*, Fig. SA7, second row) displays a pseudosquare

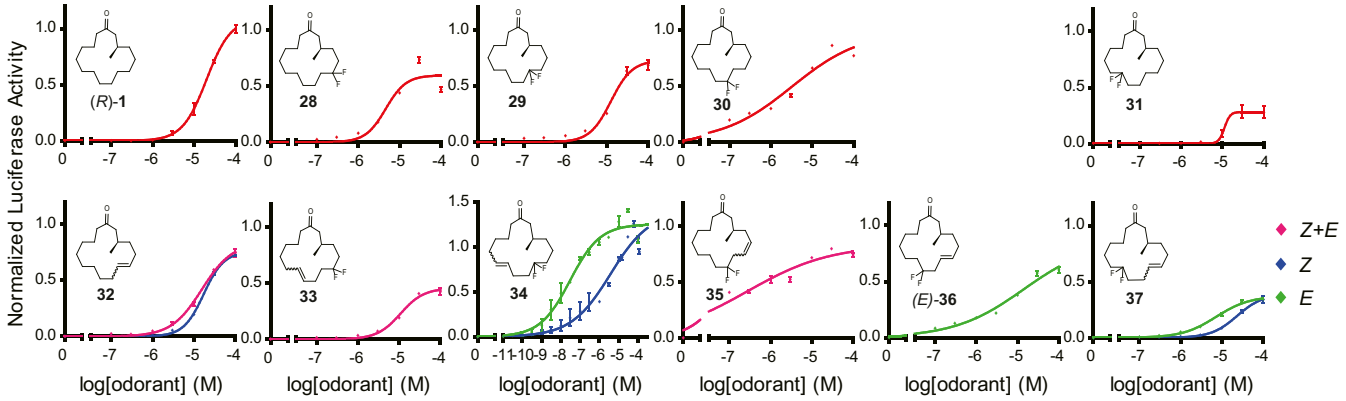

Fig. 4. Response of OR5AN1 to fluorinated (*R*)-muscone–related analogs. The responses are normalized to the highest value of (*R*)-muscone.

conformation (62). Isomer (*Z*)-**34** (EC_{50} 3.8 μM) was much more similar in potency to **1** (EC_{50} 14.2 μM) and (*R*)-**1**.

Homology Model and Docking Results. Fig. 5*A* shows the homology structural model of OR5AN1. The model was built by using the X-ray crystal structure of the human M2 muscarinic receptor (63) as a template (*SI Appendix*, Fig. S4*A*), as reported for mouse OR MOR244-3 (64, 65). Both models share some common structural features, including the disulfide bond between amino acid residues Cys98 (C98) and Cys180 (C180; Fig. 5*A*, purple). Fig. 5*B* shows the homology model of OR1A1 where the disulfide bond forms between Cys97 (C97) and Cys179 (C179). The Multiple Sequence Viewer tool as implemented in Maestro was utilized to analyze the sequence similarity between OR5AN1 and OR1A1. The default setting in pairwise sequence alignment was used; we found 58% sequence similarity between OR5AN1 and OR1A1. The sequence similarity of these two ORs is shown in *SI Appendix*, Fig. S4*B*. Note that the binding site for these musk-smelling compounds is near the extracellular loop (ECL2, at the periphery) of both receptors (Fig. 5 *A* and *B*), in contrast to the deep binding site proposed for smaller odorants in the ORI7, OR2AG1, MOR244-3, and OR-EG receptors (49, 50, 64–67). The binding site of OR5AN1 consists of Tyr260 and Phe252 of transmembrane α-helix 6 (TM6), Phe207 of transmembrane α-helix 5 (TM5), Phe105 of transmembrane α-helix 3 (TM3), and Phe194 of extracellular loop 2, while the binding site of OR1A1 consists of Tyr258 and Tyr251 of transmembrane α-helix 6 (TM6), Ile205 and Phe206 of transmembrane α-helix 5 (TM5), and Ile105 and Tyr113 of transmembrane α-helix 3 (TM3) and Leu184 of extracellular loop 2. Residue arrangements of OR5AN1 and OR1A1 are given in *SI Appendix*, Fig. S4*C*, showing the seven-transmembrane region marked in a red rectangular box.

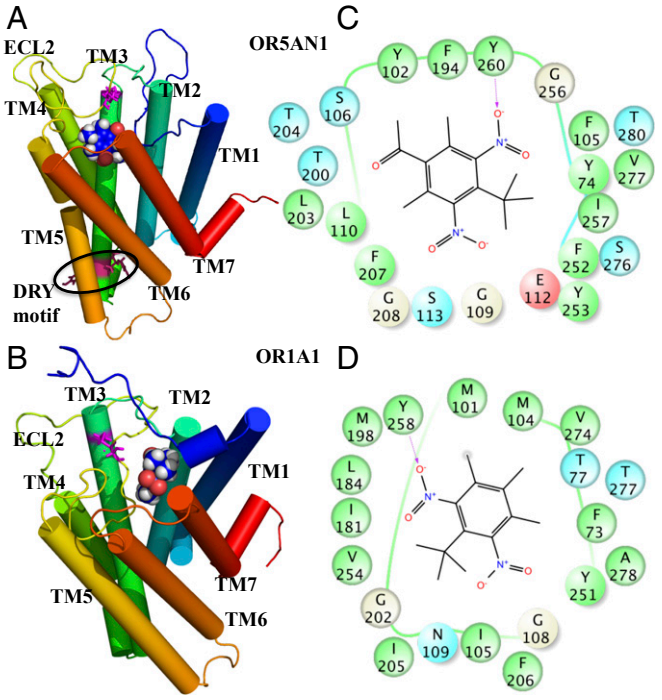

Fig. 5. Side view of the homology model (*A*) OR5AN1 and (*B*) OR1A1 including seven-transmembrane α-helices (color key: TM1, blue; TM2, light blue; TM3, light green; TM4, green; TM5, yellow; TM6, orange; and TM7, red); the odorant (shown as space-filling models) binds at the periphery of the receptor, near the extracellular loop 2 ECL2, by H-bonding to Tyr260 in OR5AN1 and to Tyr258 in OR1A1. The circled region indicates the presence of the conserved DRY motif at sites Asp122, Arg123 and Tyr124 in OR5AN1. The magenta color stick represents the disulfide bond between Cys98 and Cys180 in OR5AN1 (*A*) and between Cys97 and Cys179 in OR1A1 (*B*). (*C*) Ligand–protein interactions of musk ketone with the polar (blue) and hydrophobic (green) residues, including the H-bonding interaction (dashed magenta lines) with Tyr260 are shown. (*D*) OR1A1 binds musk tibetene by H-bonds with Tyr258 in the binding site (one-letter amino acid codes used).

The docking results show that all odorants bind by hydrogen bonding to amino acid residue Tyr260, in transmembrane α-helix 6 (TM6), at a binding pocket surrounded by aromatic, polar and nonpolar residues in OR5AN1 (Fig. 5*C* and *SI Appendix*, Fig. S5). We have analyzed docking of nitromusks, macrocyclic musks, and fluorinated musks for which OR5AN1 shows significant response. The results show that ambretone **10** binds with a high docking score (−7.28), whereas thiacyclopentadecane 1-oxide **5** has the weakest binding (docking score −5.62) among the macrocyclic compounds (*SI Appendix*, Table S5). The fluorinated musks also bind to Tyr260 with good binding scores: **30** shows the highest docking score (−7.42) while (*Z*)-**34** displays the lowest docking score (−6.72) among the fluorinated musk compounds (*SI Appendix*, Table S5). The nitro compounds show similar scores (∼ −5.60). The docking poses show that one of the nitro groups is typically involved in H-bonding with Tyr260 for all nitromusk odorants. In addition to the H-bond with Tyr260, some compounds exhibit hydrophobic interactions with surrounding phenylalanine residues (Fig. 5*C* and *SI Appendix*, Fig. S5). The docking results of the *S*-enantiomers of musk ligands show similar binding sites but do not show much difference in binding scores (*SI Appendix*, Fig. S5*G* and Table S5), probably because of protein rigidity in the docking calculation.

We also performed docking studies for OR1A1 using three active odorants, namely, musk ambrette, musk tibetene, and musk xylene. The docking studies revealed that Tyr258 and a few other hydrophobic residues such as Tyr251, Ile205, and Phe206 are very important in odorant binding. *SI Appendix*, Fig. S5*H* shows the docking results of these three odorants in OR1A1. The odorant binding pocket consists of Tyr258 and Tyr251 with surrounding polar and nonpolar residues (Fig. 5*D*). Musk ambrette **22** and musk tibetene **21** form H-bonds with Tyr258. In addition to H-bonds with Tyr258, the ligands display hydrophobic interactions with surrounding nonpolar residues such as Ile105, Tyr251, and Phe206 (Fig. 5*D*).

QM/MM Calculations. The QM/MM structural models show that macrocyclic ketones, fluorinated musks, and nitromusks are stabilized in the binding pocket of OR5AN1 by specific hydrogen-bonding interactions and favorable hydrophobic contacts. The odorant keto or nitro functional groups form H-bonds with the OH of amino acid residue Tyr260 in TM6 (Fig. 6). In addition, three phenylalanines (Phe105, Phe194, and Phe252) surrounding the odorants stabilize the odorants by establishing favorable nonpolar interactions (Fig. 6*B* and *SI Appendix*, Fig. S6). Interestingly, we found that the nitro group of musk ketone **19** forms an extra H-bond with its nearest water molecule which is also bonded to another water molecule by an H-bond. This interaction might provide extra stability in the binding site. However, the macrocyclic musks do not show any direct H-bonds with any water molecule. The QM/MM relative binding energies of the odorants correlate with the relative response of OR5AN1 toward each of these ligands. The r^2 value of the correlation is 0.78, which shows an excellent goodness of fit of the model (*SI Appendix*, Fig. S7).

Nitromusks exhibit much higher binding energies compared with macrocyclic odorants. Musk ketone **19**, musk xylene **20**, and musk tibetene **21** bind more favorably than isomuscone **8** (cyclohexadecanone) by −8.2 kcal/mol, −7.3 kcal/mol, and −5.6 kcal/mol, respectively, consistent with the experimental activity profile. Isomuscone **8** exhibits the lowest binding energy

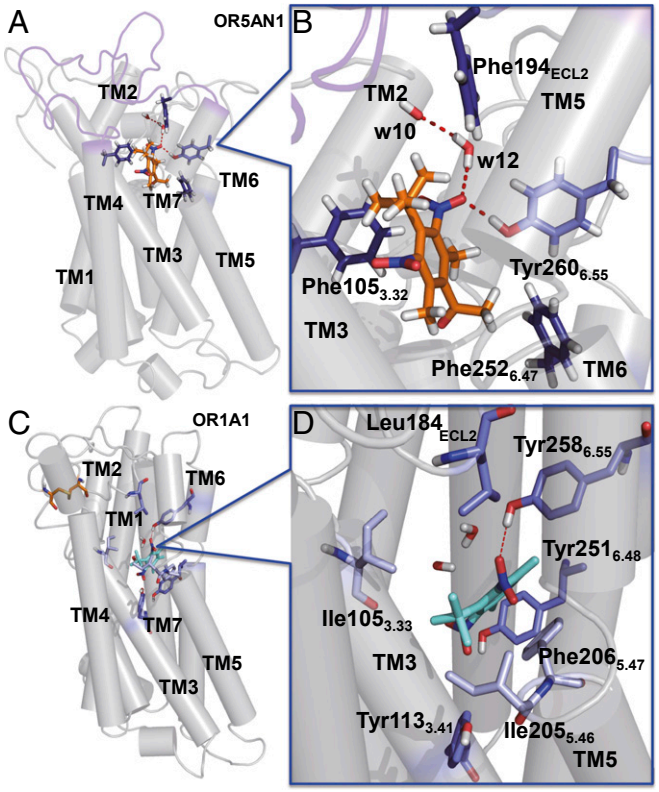

Fig. 6. (*A*) Binding site of OR5AN1. The light purple color represents the extracellular loop (ECL2). (*B*) Musk ketone bound by H-bonding to Tyr260 (TM6) and one water molecule in the OR5AN1 as modeled by density functional theory QM/MM. Color code: orange, musk ketone; light blue,Tyr260; and dark blue, three phenylalanine residues (Phe105, Phe194, and Phe252) around 4.0 Å. (*C*) Binding site of OR1A1. (*D*) Musk tibetene bound by H-bonding to Tyr258 (blue, Tyr258). The hydrophobic residues around 4.0 Å (Ile105, Ile184, Tyr113, Ile205, Phe206, and Tyr251) are shown in light blue. The corresponding Ballesteros–Weinstein numberings are shown in the subscript.

compared with other macrocyclic ligands. Among the macrocyclic ligands, ω-pentadecalactone **9** (cyclopentadecaolide) shows a relatively high binding energy, which is −5.2 kcal/mol higher than that of isomuscone **8**. In addition, we find that musk ketone **19** and musk xylene **20** bind more favorably than musk tibetene **21** by −2.6 kcal/mol and −1.7 kcal/mol, respectively. Among fluorinated musks, **28** shows higher binding energy while (*Z*)-**37** exhibits lower binding energy compared with other fluorinated musk compounds. Musk **28** binds more favorably than (*Z*)-**37** by −8.24 kcal/mol. The corresponding binding energy profiles are shown in Table 1.

We also find that (*R*)-**1** binds more favorably than (*S*)-**1** by −1.39 kcal/mol (Table 1), a result that suggests chiral selectivity of OR5AN1 toward muscone enantiomers, analogous to the selectivity reported for the MOR215-1 receptor, and consistent with the above noted lower odor human detection threshold of (*R*)-**1** compared with (*S*)-**1** (41, 68). Similarly, fluorinated musks (*R*, *E*)-**34** and (*R*)-**30** show more favorable binding than (*S*, *E*)-**34** and (*S*)-**30** by −1.72 kcal/mol and −1.94 kcal/mol, respectively (Table 1).

The QM/MM structural models show that musk tibetene **21**, musk xylene **20**, and musk ambrette **22** are stabilized in the binding pocket of OR1A1 by hydrogen-bonding interactions and favorable hydrophobic contacts. The odorant nitro functional group form H-bonds with the OH of amino acid residue Tyr258 in TM6 (Fig. 6*C*). Both Tyr258 and Tyr251, along with Ile105 and Phe206, have hydrophobic interactions with the aromatic ring of the ligands. The QM/MM models indicate that musk xylene **20** shows much higher binding energies compared with musk tibetene **21** and musk ambrette **22**. Musk xylene **20** binds more favorably than musk tibetene **21** and musk ambrette **22** by −6.04 kcal/mol and −9.92 kcal/mol, respectively (Table 1).

As with the docking calculation we found that all of the odorants show an H-bond with Tyr260 with a distance of about 1.95 Å in OR5AN1. We also observed that hydrophobic residues such as Phe105, Phe194, Phe207, and Phe252 are situated around the ligand. The closest distance between the ligand (hydrogen) and the aromatic ring (carbon) of those residues is about 4.00 Å. However, this distance reduces to 3.50 Å upon QM/MM calculation as shown in *SI Appendix*, Fig. S8. In addition, we found that water forms an H-bond with Tyr260 as well as ligands (O of nitro group, Fig. 6). However, we did not find any changes of the H-bond distance (from Tyr260 and ligand) after forming another H-bond with a water molecule. The residues surrounding the ligand shrink upon the QM/MM calculation due to the interactions of ligand and surrounding residues. Similar effects are also observed with OR1A1.

MD Simulations of OR5AN1. MD simulations show the robustness of the underlying fundamental interactions under normal room-temperature conditions. The analysis of MD simulations is based on the QM/MM model of OR5AN1, shown in Fig. 7*A*, inserted in a lipid bilayer and equilibrated at 323 K. The analysis provides insights into geometrical distortions and conformational fluctuations

Table 1. Calculated QM/MM binding energy profile of the musk odorants

Odorant receptor	Odorants	Binding energy, kcal/mol	EC_{50}, μM
OR5AN1	19	−54.97	0.02
	20	−54.08	1.28
	21	−52.32	1.74
	12	−50.77	3.43
	9	−51.97	4.78
	11	−51.13	5.23
	2	−49.27	7.32
	3	−50.56	9.05
	10	−48.92	9.15
	5	−50.00	10.58
	(*R*)-1	−48.45	19.94
	(*S*)-1	−47.06	—
	8	−46.76	19.0
	28	−53.62	4.63
	33	−49.89*	10.75
	29	−48.03	12.56
	(*Z*)-34	−49.54	3.77
	(*R*,*E*)-34	−52.91	0.03
	(*S*,*E*)-34	−51.20	—
	(*R*)-30	−53.09	3.23
	(*S*)-30	−51.15	—
	35	−52.71*	0.27
	(*E*)-36	−48.29	14.07
	31	−49.61	11.20
	(*E*)-37	−48.36	7.22
	(*Z*)-37	−45.38	23.33
	32	−46.59*	15.47
	(*Z*)-32	−47.55	17.25
OR1A1	21	−49.39	16.67
	20	−55.44	15.71
	22	−45.52	7.69

*For QM/MM modeling, the (*E*)-conformer for **32** and **33** were used. For **35** we used the (*Z*)-conformer. The names and structures for the compounds can be found in Figs. 1 and 3.

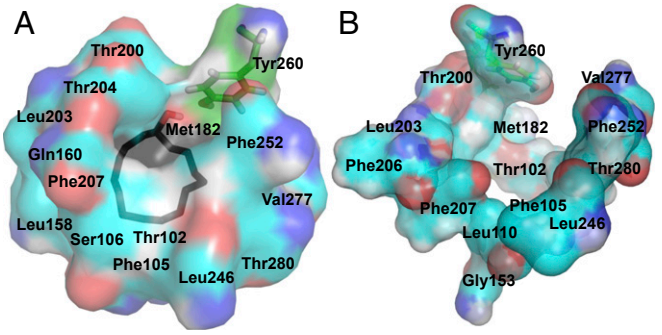

Fig. 7. Hydrophobic and aromatic residues that form the binding pocket of OR5AN1 with (*A*) and without (apo) (*B*) the odorant [cyclopentadecanol (**3**) in black stick]. Color key: hydrophobic residues (cyan) and Tyr260 (green).

(51, 69), including structural rearrangements of TM domains upon ligand binding, and on the nature of hydrophobic and H-bonding interactions responsible for ligand-binding (70–73). Specifically, 200-ns MD simulations show that macrocyclic compounds, such as (*R*)- or (*S*)-muscone [(*R*)- or (*S*)-**1**], cyclopentadecanone **2**, and ω-pentadecalactone **9**, remain bound at the proposed binding site, although they undergo significant conformational fluctuations in the binding pocket. The carbonyl groups of these macrocyclic ketones form H-bonds with several partners during the MD simulation, including Tyr260 in TM6, Ser113 in TM3, and bound water molecules at the binding site (Fig. 7 and *SI Appendix*, Figs. S9 and S10).

The percentage of MD simulation time with different odorants that establish H-bonds with specific amino acid residues at the binding pocket is shown in *SI Appendix*, Fig. S10. Interestingly, the MD simulations also show that Tyr260 functions as an "aromatic cap" by blocking the odorant exit, stabilizing the ligand at the binding site, and establishing H-bonds with Ser276 in TM7. In addition, the simulations show stabilization of odorants by interactions with aromatic and hydrophobic residues, including Tyr102, Phe105, Leu110, Phe195, Leu203, Phe207, Tyr253, and Tyr279 from the TM3, TM5, TM6, and TM7 domains (Fig. 7 and *SI Appendix*, Fig. S10). MD simulations of apo OR5AN1 (i.e., odorant-depleted OR5AN1) allowed us to analyze conformational changes of amino acid side chains induced upon odorant binding. Simulation analysis indicates that side chains of hydrophobic residues become randomly oriented in the absence of odorant (Fig. 7*B*). Upon odorant binding, however, the hydrophobic residues reorient and may induce dehydration (71) of the binding pocket (Fig. 7*A*).

Crucial Sites in OR5AN1 and OR1A1 Involved in the Binding of Musk-Smelling Compounds. Computational analysis has enabled us to design site-directed mutagenesis experiments that provide further insight into the roles of key amino acid residues, as probed by measurements of the receptor activation, and support for the structural model of the binding site. We have expressed and analyzed the mutant Tyr260Phe of OR5AN1, which completely abolished the receptor response to macrocyclic musks, nitromusks, and fluorinated musks relative to wild-type OR5AN1 (Fig. 8 and *SI Appendix*, Fig. S11). We have also analyzed the mutant Tyr279Ala of OR5AN1, since the MD simulations showed evidence of cyclopentadecanone **2** interacting not only with Tyr260 but also with Tyr279 (*SI Appendix*, Fig. S10). We find that the mutation Tyr279Ala also dramatically affects the receptor response to **2** (*SI Appendix*, Fig. S12), consistent with the structural model of the binding site where Tyr279 establishes important interactions that are critical for odorant binding.

For OR1A1, we expressed and analyzed mutants Tyr258Phe and Tyr251Phe. Both mutants completely abolished the receptor response to musk tibetene **21** and musk xylene **20**

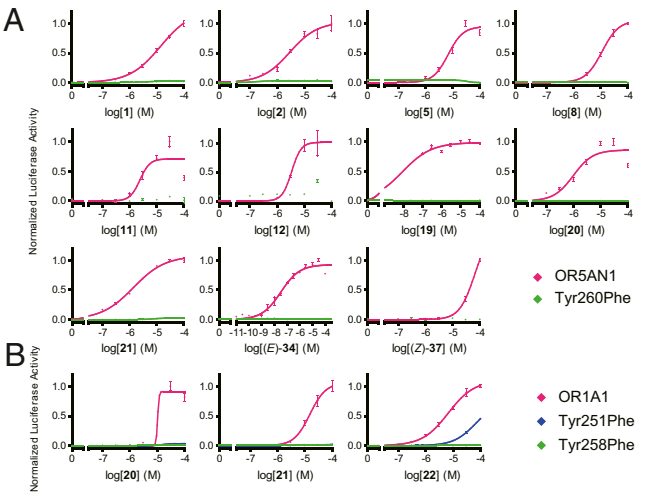

Fig. 8. Responses of human musk receptor active-site mutants to corresponding musk-smelling ligands. (*A*) Responses of OR5AN1 active-site mutants to macrocyclic musks (**1**, **2**, **5**, **8**, **11**, and **12**), nitromusks (**19**–**21**), and fluorinated musks [(*E*)-**34**, (*Z*)-**37**]. (*B*) Responses of OR1A1 active-site mutants to nitromusks (**20**–**22**). Responses are normalized to responses of the wild-type receptor to each ligand.

relative to wild-type OR1A1 (Fig. 8). The Tyr258Phe mutant completely abolished the receptor response to musk ambrette **22** while the Tyr251Phe mutant demonstrated decreased receptor response.

It is possible that the mutations in OR5AN1 and OR1A1 may affect receptor trafficking or protein stability, thus causing the loss-of-function phenotypes. We therefore evaluated the cell-surface membrane expression of these mutants in Hana3A cells by flow cytometry. We found that mutations Tyr260Phe/Tyr279Ala and Tyr251Phe/Tyr258Phe did not significantly alter the receptors' surface expression relative to wild-type OR5AN1 and OR1A1, respectively. Thus, sites Tyr260 and Tyr258 may be critical for receptor function, as suggested by our computational structural models of the OR5AN1 and OR1A1 binding sites.

Three-Dimensional Quantitative Structure–Activity Relationships (3D-QSAR) Model: Atom-Based QSAR Model. We built a 3D-QSAR model to determine the extent that electron withdrawing/HB-acceptor moieties, hydrophobic, and other atom types in the odorants influence binding response in OR5AN1. In this context, an atom-based 3D-QSAR model was generated to investigate the correlation between binding activity and different atom types in the odorants. A four-component model with good statistics was observed with a significant regression coefficient, r^2, of 0.93 (Fig. 9). The regression coefficient for test set q^2 was found to be

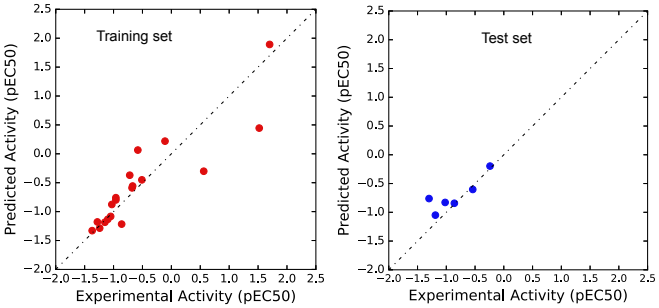

Fig. 9. Atom-based QSAR model. Experimental pEC_{50} vs. calculated pEC_{50} for the training and test sets.

0.67. Other statistical parameters such as SD, F value, root-mean-square error (RMSE), and Pearson r were 0.25, 68.90, 0.21, and 0.85, respectively. A report showed that the performance of Phase is good when $q^2 > 0.7$ or $r^2 > 0.4$ (74). This report also mentioned that low SD and RMSE and high F value and Pearson r indicate a more statistically significant regression. It is worth noting that all of these parameters are very significant in the developed QSAR model.

The training and test-set molecules are listed in *SI Appendix*, Table S6. According to the model, four components, namely hydrophobic/nonpolar part and H-bond acceptor groups/atoms, negative ionic and positive ionic, are affecting the response of the musk receptors to the odorants. Among these components, the hydrophobic/nonpolar part contributes 77% and H-bond acceptors group/atoms 13%, while both negative ionic and positive ionic atoms influence 10%. This study is also confirmed by mapping of binding sites created by SiteMap in Schrodinger's Maestro V. 10.2.010 software package. SiteMap reveals that the binding site is mostly hydrophobic along with some polar residues (*SI Appendix*, Fig. S14). Therefore, the hydrophobic/nonpolar interaction is also expected to contribute to ligand binding in addition to H-bond interaction.

We have introduced structural models of OR5AN1 and OR1A1 supported by site-directed mutagenesis and measurements of activity profiles, providing valuable insights into the nature of musk odorant–receptor interactions. We have shown that nitromusks exhibit high response compare with macrocyclic compounds, while the 15-membered thiacyclopentadecane 1-oxide **5** also proved to be active, despite the fact that the sulfinyl group is pyramidal while the carbonyl group is planar. We found that compound (*E*)-**34**, containing a CF_2 group and (*E*)-olefin as conformational constraints, is the most potent agonist of a series of CF_2-containing muscones. Along with the H-bond acceptor, the hydrophobicity of the musk compounds also influenced odorant response. Our findings are consistent with the proposed involvement of TM6 during activation of GPCRs (75–78). Generated 3D-QSAR models also confirm that both H-bond acceptor and nonpolar parts of the odorants affect the response to OR5AN1.

The significant differences seen in the IR spectra of the macrocyclic ketones, the nitromusks, and thiacyclopentadecane 1-oxide **5**, all of which are good-to-excellent ligands for OR5AN1, provide further evidence for the implausibility of the vibrational theory of olfaction (39), in accord with other recent reports (79–82). Furthermore, the various therapeutic activities of musk compounds have yet to be linked to their respective drug targets in vivo. One possibility is that these compounds may function through the group of ectopically expressed ORs in tissues of nonolfactory origins (83–86). Alternatively, as members of the GPCR superfamily, ORs may share structural and mechanistic similarities with pharmacophore GPCRs from other subclasses. Thus, understanding the active sites for musk-responsive ORs may be instructive in the study of the pharmacological effects of muscone and related compounds involving non-OR GPCRs.

Materials and Methods

Chemicals. Macrocyclic musks, polycyclic musks, nitromusks, and musk-related odorants studied were obtained from commercial sources, with the exception of civetone **12**, dihydrocivetone **11**, thiacyclotridecane 1-oxide **17**, and thiacyclopentadecane 1-oxide **5**, which were prepared by standard methods from known precursors (*SI Appendix*); synthesis of saturated and unsaturated fluorinated musks was done as previously described (62). Procedures and spectroscopic characterization are given in *SI Appendix*.

Cloning and Mutagenesis. OR5AN1 and OR1A1 and an N-terminal rhodopsin tag were cloned into the pCI mammalian expression vector, as described previously (87). OR5AN1 site-directed mutagenesis was carried out using overlap extension PCR. The identities of all constructs were confirmed by sequencing.

Cell Culture, Luciferase, and GloSensor cAMP Assays. An HEK293T-derived Hana3A cell line was grown in Minimum Essential Medium (HyClone) containing 10% FBS at 37 °C with 5% CO_2. For the luciferase assay, after 18–24 h, OR or mutant receptor, the accessory factor, mRTP1S, and constructs for firefly luciferase and Renilla luciferase expression were transfected into cells for luciferase assay. For the GloSensor cAMP assay, OR, mRTP1S, and a GloSensor plasmid were transfected into cells. Lipofectamine 2000 (Invitrogen) was used for transfection. Twenty-four hours after transfection, the cells were stimulated with odorants dissolved in CD293 (Invitrogen) for the luciferase assay or HBSS for the GloSensor cAMP assay.

Other materials and methods can be found in *SI Appendix*.

ACKNOWLEDGMENTS. V.S.B. thanks the National Energy Research Scientific Computing Center for computational time. This work was supported by NSF Grant CHE-1265679 and NIH Grant 5R01 DC014423 (subaward) (to E.B.), NIH Grant 5R01 DC014423 (to H.M.), the European Research Council and the Engineering Science Research Council (D.O.), Research Support Foundation of the State of São Paulo and Brazilian National Council of Scientific and Technological Development (R.A.C.), the Chinese Scholarship Council for studentship support (M.Y.), NSF Grant 31070972 (to H.Z.), Science and Technology Commission of Shanghai Municipality Grant 16ZR1418300 (to H.Z.), Shanghai Eastern Scholar Program Grant J50201 (to H.Z.), and NIH Grant 1R01GM106121–01A1 (to V.S.B.).

1. Ohloff G, Pickenhagen Q, Kraft P (2012) *Scent and Chemistry. The Molecular World of Odors* (Wiley-VCH, Weinheim, Germany).
2. Ruzicka L (1926) Carbon rings. I. Constitution of civetone. *Helv Chim Acta* 9:230–248.
3. Garrec K, Fletcher SP (2016) $Cp_2ZrMeCl$: A reagent for asymmetric methyl addition. *Org Lett* 18:3814–3817.
4. Shen J, Shi Y, Tian W (2015) Synthesis of (*R*)-(–)-muscone from (*R*)-5-bromo-4-methylpentanoate: A chiron approach. *Chin J Chem* 33:683–687.
5. Zou Y, et al. (2014) A novel oxy-oxonia(azonia)-cope reaction: Serendipitous discovery and its application to the synthesis of macrocyclic musks. *Chem Biodivers* 11: 1608–1628.
6. Sell CS (2014) *Chemistry and the Sense of Smell* (Wiley, Hoboken, NJ).
7. Chapuis C, Robvieux F, Cantatore C, Saint-Leger C, Maggi L (2012) Exaltone (*R*) (=cyclopentadecanone) from isomuscone (*R*) (=cyclohexadecanone), a one-C-atom ring-contraction methodology via a stereospecific Favorskii rearrangement: Regioselective application to (–)-(*R*)-muscone. *Helv Chim Acta* 95:428–447.
8. Sun X, Yu F, Ye T, Liang X, Ye J (2011) Catalytic asymmetric Michael reactions of α,β-unsaturated ketones with sulfonyl-containing nucleophiles: Chiral synthesis of (*R*)-muscone and (*S*)-celery ketone. *Chemistry* 17:430–434.
9. Fehr C, Buzas AK, Knopff O, de Saint Laumer JY (2010) (+)-(*R*,*Z*)-5-Muscenone and (–)-(*R*)-muscone by enantioselective aldol reaction and Grob fragmentation. *Chemistry* 16:2487–2495.
10. Matsuda H, Tanaka S, Yamamoto K, Ishida K (2008) Synthesis of *l*-muscone by asymmetric methylation via enol esters. *Chem Biodivers* 5:1023–1033.
11. Erden I, Cao W, Price M, Colton M (2008) A three-carbon (n+1+2) ring expansion method for the synthesis of macrocyclic enones. Application to muscone synthesis. *Tetrahedron* 64:5497–5501.
12. Knopff O, Kuhne J, Fehr C (2007) Enantioselective intramolecular aldol addition/dehydration reaction of a macrocyclic diketone: Synthesis of the musk odorants (*R*)-muscone and (*R*,*Z*)-5-muscenone. *Angew Chem Int Ed Engl* 46:1307–1310.
13. Sell CS (2006) On the unpredictability of odor. *Angew Chem Int Ed Engl* 45: 6254–6261.
14. Ito M, Kitahara S, Ikariya T (2005) CpRu(PN) complex-catalyzed isomerization of allylic alcohols and its application to the asymmetric synthesis of muscone. *J Am Chem Soc* 127:6172–6173.
15. Guo Y, Wu XL, Li JL, Xu RQ, Shi Z (2005) Novel synthetic method for muscone. *Synth Commun* 35:2489–2494.
16. Ruedi G, Hansen HJ (2004) Cyclopropylcarbinyl radicals as three-carbon insertion units: Easy synthesis of C-15 macrocyclic ketones by three-carbon ring expansion. *Tetrahedron Lett* 45:5143–5145.
17. Scafato P, Cunsolo G, Labano S, Rosini C (2004) Asymmetric activation of tropos catalysts in the stereoselective catalytic conjugate additions of R_2Zn to α,β-enones: An efficient synthesis of (–)-muscone. *Tetrahedron* 60:8801–8806.
18. Fehr C, Galindo J, Etter O (2004) An efficient enantioselective synthesis of (+)-(*R*,*Z*)-5-muscenone and (–)-(*R*)-muscone–An example of a kinetic resolution and enantioconvergent transformation. *Eur J Org Chem* 2004:1953–1957.
19. Fehr C, Galindo J, Farris I, Cuenca A (2004) Efficient synthesis of (–)-(*R*)-muscone by enantioselective protonation. *Helv Chim Acta* 87:1737–1747.
20. Scafato P, Labano S, Cunsolo G, Rosini C (2003) Catalytic enantioselective conjugate addition of dialkyl zinc reagents to α,β-unsaturated ketones mediated by new phosphite ligands containing binaphthalene/1,2-diphenylethane moieties: A practical synthesis of (*R*)-(–)-muscone. *Tetrahedron Asymmetry* 14:3873–3877.

21. Nagel M, Hansen HJ, Frater G (2002) Short and versatile two-carbon ring expansion reactions by thermo-isomerization: Novel straightforward synthesis of (±)-muscone, nor- and homomuscones, and further macrocyclic ketones. *Synlett* 2002:280–284.
22. Fujimoto S, Yoshikawa K, Itoh M, Kitaharai T (2002) Synthesis of (*R*)- and (*S*)- muscone. *Biosci Biotechnol Biochem* 66:1389–1392.
23. Baur A (1891) Studien uber den kunstlichen moschus. *Ber Dtsch Chem Ges* 24: 2832–2843.
24. Homem V, Magalhães I, Alves A, Santos L (2017) Assessing seasonal variation of synthetic musks in beach sands from Oporto coastal area: A case study. *Environ Pollut* 226:190–197.
25. van der Burg B, et al. (2008) Endocrine effects of polycyclic musks: Do we smell a rat? *Int J Androl* 31:188–193.
26. Cen W, Chen Z, Gu N, Hoppe R (2017) Prevention of AMI induced ventricular remodeling: Inhibitory effects of heart-protecting musk pill on IL-6 and TNF-α. *Evid Based Complement Alternat Med* 2017:3217395.
27. Feng Q, Liu J (2015) Progress on pharmacological activity of muscone. *Food Drug* 17: 212–214.
28. Zhang XZ, Hou YM, Ou ZH (2014) [Effect of Shexiang Baoxin pill on coronary vasodilation by analysis of coronary angiography]. *Zhongguo Zhong Xi Yi Jie He Za Zhi* 34: 1432–1435.
29. Wang X, et al. (2014) Beneficial effects of muscone on cardiac remodeling in a mouse model of myocardial infarction. *Int J Mol Med* 34:103–111.
30. Liang QQ, Zhang M, Zhou Q, Shi Q, Wang YJ (2010) Muscone protects vertebral endplate degeneration by antiinflammatory property. *Clin Orthop Relat Res* 468: 1600–1610.
31. Liang H, Chen H, Gao Y, Cai D (2003) Effect of muscone on neuronal glutamate transporter EAAC1 expression in rats with acute cerebral ischemia. *Chin J Integr Med* 9:285–288.
32. Huang M, et al. (2016) Identification and quantification of the anti-inflammatory constituents in Pian-Tze-Huang by liquid chromatography combined with quadrupole time-of-flight and triple quadrupole mass spectrometry. *J Chromatogr B Analyt Technol Biomed Life Sci* 1027:27–39.
33. Asada R, Kageyama K, Tanaka H, Saitoh Y, Miwa N (2012) Antitumor and antiinvasive effects of diverse musk-fragrant macrocyclic ketones and their enhancement by hyperthermia. *Mol Med Rep* 5:148–152.
34. Kato M (2004) The stimulatory effect on the secretion of the female sex hormone by some perfumery raw materials. *Fragrance J* 32:56–60.
35. Zhang CG, Wang H, Zhao BS, Ye LQ (1982) Effects of synthetic muskone on early pregnancy in mice. *Acta Zool Sinica* 28:242–244.
36. Gane S, et al. (2013) Molecular vibration-sensing component in human olfaction. *PLoS One* 8:e55780.
37. Nara K, Saraiva LR, Ye X, Buck LB (2011) A large-scale analysis of odor coding in the olfactory epithelium. *J Neurosci* 31:9179–9191.
38. Sato-Akuhara N, et al. (2016) Ligand specificity and evolution of mammalian musk odor receptors: Effect of single receptor deletion on odor detection. *J Neurosci* 36: 4482–4491.
39. Block E, et al. (2015) Implausibility of the vibrational theory of olfaction. *Proc Natl Acad Sci USA* 112:E2766–E2774.
40. McClintock TS, et al. (2014) In vivo identification of eugenol-responsive and muscone-responsive mouse odorant receptors. *J Neurosci* 34:15669–15678.
41. Shirasu M, et al. (2014) Olfactory receptor and neural pathway responsible for highly selective sensing of musk odors. *Neuron* 81:165–178.
42. Niesen MJM, Bhattacharya S, Vaidehi N (2011) The role of conformational ensembles in ligand recognition in G-protein coupled receptors. *J Am Chem Soc* 133: 13197–13204.
43. Goldfeld DA, Zhu K, Beuming T, Friesner RA (2011) Successful prediction of the intra- and extracellular loops of four G-protein-coupled receptors. *Proc Natl Acad Sci USA* 108:8275–8280.
44. Ranzani M, et al. (2017) Revisiting olfactory receptors as putative drivers of cancer. *Wellcome Open Res* 2:9.
45. Park JH, et al. (2013) Opsin, a structural model for olfactory receptors? *Angew Chem Int Ed Engl* 52:11021–11024.
46. Gaillard I, Rouquier S, Giorgi D (2004) Olfactory receptors. *Cell Mol Life Sci* 61: 456–469.
47. Kim SK, Goddard WA, 3rd (2014) Predicted 3D structures of olfactory receptors with details of odorant binding to OR1G1. *J Comput Aided Mol Des* 28:1175–1190.
48. Topin J, et al. (2014) Discrimination between olfactory receptor agonists and non-agonists. *Chemistry* 20:10227–10230.
49. Gelis L, Wolf S, Hatt H, Neuhaus EM, Gerwert K (2012) Prediction of a ligand-binding niche within a human olfactory receptor by combining site-directed mutagenesis with dynamic homology modeling. *Angew Chem Int Ed Engl* 51:1274–1278.
50. Kurland MD, et al. (2010) Discrimination of saturated aldehydes by the rat I7 olfactory receptor. *Biochemistry* 49:6302–6304.
51. Floriano WB, Vaidehi N, Goddard WA, 3rd, Singer MS, Shepherd GM (2000) Molecular mechanisms underlying differential odor responses of a mouse olfactory receptor. *Proc Natl Acad Sci USA* 97:10712–10716.
52. Sommer C (2004) *The Handbook of Environmental Chemistry* (Springer, New York).
53. Müller A, Schütz AF (1938) Polymembered cyclic compounds. X. Dodecamethylene sulfide, tridecamethylene sulfide and tetradecamethylene sulfide. *Chem Ber* 71B: 692–695.
54. Setzer WN (2009) Conformational analysis of thioether musks using density functional theory. *Int J Mol Sci* 10:3488–3501.
55. Goeke A (2002) Sulfur-containing odorants in fragrance chemistry. *Sulfur Rep* 23: 243–278.
56. Theimer ET, Davies JT (1967) Olfaction, musk odor, and molecular properties. *J Agric Food Chem* 15:6–14.
57. Stetter H, Wirth W (1960) Zur Kenntnis der makrocyclischen ringsysteme, VI eine einfache methode zur herstellung makrocyclischer dithioäther. *Justus Liebigs Ann Chem* 631:144–147.
58. Saito H, Chi Q, Zhuang H, Matsunami H, Mainland JD (2009) Odor coding by a Mammalian receptor repertoire. *Sci Signal* 2:ra9.
59. Skibinski M, et al. (2011) Alicyclic ring structure: Conformational influence of the CF_2 group in cyclododecanes. *Angew Chem Int Ed Engl* 50:10581–10584.
60. Michel D, Schlosser M (2000) Odor-structure relationships using fluorine as a probe. *Tetrahedron* 56:4253–4260.
61. Corr MJ, et al. (2016) Fluorine in fragrances: Exploring the difluoromethylene (CF_2) group as a conformational constraint in macrocyclic musk lactones. *Org Biomol Chem* 14:211–219.
62. Callejo R, et al. (2016) Fluorinated musk fragrances: The CF_2 group as a conformational bias influencing the odour of civetone and (*R*)-muscone. *Chemistry* 22: 8137–8151.
63. Haga K, et al. (2012) Structure of the human M2 muscarinic acetylcholine receptor bound to an antagonist. *Nature* 482:547–551.
64. Sekharan S, et al. (2014) QM/MM model of the mouse olfactory receptor MOR244-3 validated by site-directed mutagenesis experiments. *Biophys J* 107:L5–L8.
65. Duan X, et al. (2012) Crucial role of copper in detection of metal-coordinating odorants. *Proc Natl Acad Sci USA* 109:3492–3497.
66. Li Y, et al. (2014) Aldehyde recognition and discrimination by mammalian odorant receptors via functional group-specific hydration chemistry. *ACS Chem Biol* 9: 2563–2571.
67. Baud O, et al. (2011) The mouse eugenol odorant receptor: Structural and functional plasticity of a broadly tuned odorant binding pocket. *Biochemistry* 50:843–853.
68. Sinqh A, Mehrotra A, Regen SL (1981) High yield medium ring synthesis of thiacycloalkanes. *Synth Commun* 11:409–411.
69. Karplus M, Kuriyan J (2005) Molecular dynamics and protein function. *Proc Natl Acad Sci USA* 102:6679–6685.
70. Charlier L, et al. (2012) How broadly tuned olfactory receptors equally recognize their agonists. Human OR1G1 as a test case. *Cell Mol Life Sci* 69:4205–4213.
71. Dror RO, et al. (2011) Pathway and mechanism of drug binding to G-protein-coupled receptors. *Proc Natl Acad Sci USA* 108:13118–13123.
72. Klepeis JL, Lindorff-Larsen K, Dror RO, Shaw DE (2009) Long-timescale molecular dynamics simulations of protein structure and function. *Curr Opin Struct Biol* 19: 120–127.
73. Wolf S, Böckmann M, Höweler U, Schlitter J, Gerwert K (2008) Simulations of a G protein-coupled receptor homology model predict dynamic features and a ligand binding site. *FEBS Lett* 582:3335–3342.
74. Evans DA, Doman TN, Thorner DA, Bodkin MJ (2007) 3D QSAR methods: Phase and catalyst compared. *J Chem Inf Model* 47:1248–1257.
75. Altenbach C, Kusnetzow AK, Ernst OP, Hofmann KP, Hubbell WL (2008) High-resolution distance mapping in rhodopsin reveals the pattern of helix movement due to activation. *Proc Natl Acad Sci USA* 105:7439–7444.
76. Hubbell WL, Altenbach C, Hubbell CM, Khorana HG (2003) Rhodopsin structure, dynamics, and activation: A perspective from crystallography, site-directed spin labeling, sulfhydryl reactivity, and disulfide cross-linking. *Adv Protein Chem* 63:243–290.
77. Farrens DL, Altenbach C, Yang K, Hubbell WL, Khorana HG (1996) Requirement of rigid-body motion of transmembrane helices for light activation of rhodopsin. *Science* 274:768–770.
78. Sheikh SP, Zvyaga TA, Lichtarge O, Sakmar TP, Bourne HR (1996) Rhodopsin activation blocked by metal-ion-binding sites linking transmembrane helices C and F. *Nature* 383:347–350.
79. Muthyala RS, Butani D, Nelson M, Tran K (2017) Testing the vibrational theory of olfaction: A bio-organic chemistry laboratory experiment using Hooke's law and chirality. *J Chem Educ* 94:1352–1356.
80. Paoli M, et al. (2017) Minute impurities contribute significantly to olfactory receptor ligand studies: Tales from testing the vibration theory. *eNeuro* 4:ENEURO.0070-0017.2017.
81. Hoehn RD, Nichols DE, McCorvy JD, Neven H, Kais S (2017) Experimental evaluation of the generalized vibrational theory of G protein-coupled receptor activation. *Proc Natl Acad Sci USA* 114:5595–5600.
82. Block E, Batista VS, Matsunami H, Zhuang H, Ahmed L (2017) The role of metals in mammalian olfaction of low molecular weight organosulfur compounds. *Nat Prod Rep* 34:529–557.
83. Chang AJ, Ortega FE, Riegler J, Madison DV, Krasnow MA (2015) Oxygen regulation of breathing through an olfactory receptor activated by lactate. *Nature* 527:240–244.
84. Pluznick JL, et al. (2013) Olfactory receptor responding to gut microbiota-derived signals plays a role in renin secretion and blood pressure regulation. *Proc Natl Acad Sci USA* 110:4410–4415.
85. Flegel C, Manteniotis S, Osthold S, Hatt H, Gisselmann G (2013) Expression profile of ectopic olfactory receptors determined by deep sequencing. *PLoS One* 8:e55368.
86. Braun T, Voland P, Kunz L, Prinz C, Gratzl M (2007) Enterochromaffin cells of the human gut: Sensors for spices and odorants. *Gastroenterology* 132:1890–1901.
87. Saito H, Kubota M, Roberts RW, Chi Q, Matsunami H (2004) RTP family members induce functional expression of mammalian odorant receptors. *Cell* 119:679–691.